Chapter 3

Optimal Operation of an Electricity-Hydrogen DC Microgrid with Integrated Demand Response

3.1 Introduction

The DCμG architecture is becoming popular for serving remote rural households and facilities, community buildings, data centres, etc. [160]. Since the capacity of controllable power generation facility is limited in a DCμG, a high proportion of RES, like SPG and WPG, introduces volatility and uncertainty in maintaining the generation-demand balance. Moreover, increasing penetration of PHEV alters the existing load demand pattern of the system. The challenge of maintaining generation demand balance with volatile RES generation can be handled by introducing flexible resources in the system. For instance, a BESS can provide renewable firming, energy balancing, and grid support services apart from providing operating economy in the form of arbitrage benefit [161]. On the consumer side, advanced metering infrastructure coupled with a conducive market mechanism leads to flexible consumers participating as DR entities, providing additional flexibility to the system operator [162]. Apart from RES, green H_2 energy has also emerged as a popular technology for decarbonisation [163]. Low-carbon and green H_2 is in demand to avoid "deep electrification", for industrial processes and the transportation sector, and can reduce carbon footprints [163]. Further, the sectoral coupling between H_2 and electricity facilitates the generation of green H_2 using P2H units with excess RES generation, stor-

age of H_2, and production of electricity from stored H_2 using H2P units during periods of high electricity costs and RES generation deficit [163]. The coordinated scheduling of a coupled H_2-electricity system improves system security and operational efficiency [76]. However, an assessment of the levelized cost of energy (LCOE) of electricity and H_2 produced by an electrolyzer using RES (WPG and concentrated photovoltaic thermal systems) revealed that economic competitiveness can be achieved for large power installations [164]. Another study on the techno-economic competitiveness of HSS for μG applications revealed that integrating H_2 and electricity sectors and replacement of diesel generators by FC reduce greenhouse gas (GHG) emissions substantially [165]. However, the capital costs of FC, electrolyzer, and HSS must be reduced by $\sim$ 50% to guarantee an economic advantage [165]. Several investigations have revealed that integration of H_2-electricity sectors within a μG is technically feasible and advantageous. However, economic competitiveness can be attained with a substantive reduction in capital costs of electrolyzer, FC, and HSS [165], the rise of fossil fuel prices [166], and for applications requiring multi-energy delivery pathways [167]. Nevertheless, electricity-H_2 sectoral coupling offers multifarious advantages like environmental benefits, enhanced power system operation flexibility, reduction in RES curtailment, flexibility of load regulation using the H_2 system, a chance to leverage complementary characteristics of BESS and HSS (BESS has high power density and HSS has high energy density with long-term storage facility). Further, with maturity of H_2 technology, the capital costs of FC, HSS, and electrolyzer will reduce in the future [78]. Also, sectoral coupling of H_2 and electricity is a feasible and attractive solution when the μG requires large "self-sufficiency ratio", and oversizing of SPG is not possible [168]. Moreover, the development and maturity of FC technology, like the "reversible solid oxide FC", will result in higher efficiency, thereby making the electricity-H_2 coupling economically competitive in the future [169]. Therefore, the study of co-optimisation and co-scheduling of electricity-H_2 μGs is a significant research problem to facilitate widespread deployment of the technology in the future and has recently gained traction with the research community. In this context, this chapter deals with the EMS of a coupled electricity-H_2 DCμG. A coordinated EMS encompassing various flexible resources on the generation and demand sides and across multiple energy vectors (electricity and H_2) for a DCμG is a challenging problem.

A detailed literature survey has been presented in **section 1.3**. A comparison of

Table 3.1: Summary of literature review.

Ref.	Objective	Uncertainty Modelling			DR	Optimisation structure	P2H	PHEV
		Input RVs	Correlation	Technique				
[17]	B+C	✗	NA	NA	✗	Centralised	✗	✗
[104]	B	✗	NA	NA	✓	Centralised	✗	✗
[51]	B	W+S+P	✗	ANN	✗	Centralised	✗	✗
[22]	B	✗	NA	NA	✗	Centralised	✗	✗
[23]	B	✗	NA	NA	✗	Centralised	✗	✗
[114]	B+G	✗	NA	NA	✗	Distributed	✗	✗
[26], [27]	H	✗	NA	NA	✗	Distributed [26], Decentralised [27]	✗	✗
[70]	B+D+E	S+L	✓	INT-Probabilistic	✗	Centralised	✗	✗
[64]	B+D+E	S+L+W	✗	Probabilistic	✗	Centralised	✗	✗
[34]	G	✗	NA	NA	✗	MPC	✗	✓
[35]	H	✗	NA	NA	✗	Distributed	✗	✗
[36]	I	✗	NA	NA	✗	Distributed	✗	✗
[66]	A+B+C	S+L	✗	Probabilistic	✗	Centralised	✗	✗
[48]	B+F	S	✗	CCP	✗	Decentralised	✗	✓
[37]	B+C+J+K+M	✗	NA	NA	✗	Centralised	✗	✗
[53]	B+K	W+L	✗	Affine adjustable policy	✗	Centralised	✗	✗
[38]	B+C+H	✗	NA	NA	✗	Centralised	✗	✗
P.W.	**B**	**W+S+L+P+T**	✓	**Copula**	✓	**Decentralised**	✓	✓

DR = Demand response. MPC = Model predictive control. P2H = Power-to-hydrogen. PHEV = Plug-in hybrid electric vehicle.
A = Small-signal stability improvement. B = Cost reduction. C = Emission reduction. D = Voltage stability improvement.
E = Current sharing accuracy. F = Reserve provision. G = Resilience. H = Loss minimisation. I = Voltage profile improvement.
J = WQoS minimisation. K = Value of curtailed energy minimisation. L = Load. M = Value of loss load minimisation. P = Grid-energy price.
S = Solar generation. T = Temperature. W = Wind generation. NA = Not applicable. P.W.= Proposed work

contributions made by relevant papers with the work done in this chapter is given in table 3.1. The following gap areas are found in the existing literature:

- **Gap#1)** While several studies on the EMS of coupled electricity-H_2 systems have been carried out, most studies pertained to AC networks or IESs, where either AC network model and constraints were considered [76], or network model and constraints (line ratings, bus voltage limits, etc.) were not considered at all [12, 74, 78, 79, 80, 81]. Therefore, the above studies on multi-energy vector coordination cannot be directly extended to a DCμG network. In other words, a separate comprehensive investigation on the EMS for a coupled electricity-H_2 DCμG considering DCμG network model and network constraints is required not only to assess the impact of the sectoral coupling on operating economy but also to guarantee that network operating constraints like line ratings and bus voltage limits are not violated.

- **Gap#2)** The DR can be implemented either using DLC or by guiding the consumption pattern of the flexible consumers by setting incentive or price-based (RPP)

schemes. The DLC scheme is often not preferred since it compromises the consumer privacy [125, 126]. The DR scheme should preferably be privacy-preserving with minimum information exchange between the DCμGO and the flexible consumers. Most studies involving DR in a DCμG considered aggregated models of DR participators without dealing with equipment-level constraints [104]. Further, most studies used incentive-based schemes with pre-decided incentive values [104] without addressing the theoretical basis for setting the incentive price of DR participation in a DCμG network. Similarly, to the author's knowledge, the theoretical basis for setting the RPP for implementing a DR scheme considering DCμG network model and constraints has not been explicitly reported. Therefore, a theoretical basis for setting the RPP considering DCμG network model and associated constraints for DR implementation in a decentralised framework (for privacy preservation) needs investigation.

- **Gap#3)** While correlation among input RVs have been considered for AC systems in the literature, the impact of correlated uncertain input RVs (wind and solar power, grid price, PHEV demand, temperature) on the EMS of a DCμG has received little focus [17, 22, 23, 26, 27, 34, 35, 36, 37, 38, 48, 51, 53, 64, 66, 104, 114]. However, the correlated input RVs should be incorporated in the DCμG EMS to mitigate the risk of dispatch strategy.

The current chapter addresses the gaps mentioned above and deals with a comprehensive probabilistic EMS for a coupled electricity-H_2 DCμG along with a decentralised privacy-preserving DR scheme considering a detailed DCμG network model and constraints. Therefore, the contributions of this chapter are as follows:

- **Contribution#1)** A privacy-preserving EMS with an RPP-based decentralised DR program is proposed for a DCμG with sectoral coupling between electricity and H_2 to maximise the profit of the DCμGO and reduce the energy usage costs of the consumers. Therefore, the first gap area is addressed.

- **Contribution#2)** The theoretical basis for setting the RPP is established considering the DCμG network model and network constraints using the concept of competitive equilibrium. Hence, the second gap area is bridged.

- **Contribution#3)** PHEV and BESS operational flexibility, the thermal inertia of buildings and electrical demand shifting potential of HSS are coordinated to form an "integrated demand response (IDR) scheme" for improving the techno-economic performance of a coupled electricity-H_2 DCμG considering the network model and network constraints.

- **Contribution#4)** The uncertainties, including correlation between input RVs, are modelled using probabilistic Copula models and incorporated into the EMS to mitigate the risk of dispatch strategy in an uncertain environment. Therefore, the third gap area is bridged.

The rest of the chapter has the following pattern. The methodology is discussed in **section 3.2**. Simulation studies and conclusions are presented in **section 3.3** and **section 3.4**, respectively.

3.2 Materials and Methods

3.2.1 System Configuration and Operation Framework

A grid-connected DCμG comprising smart buildings, WPG, SPG, BESS, MT, HSS, electrolyzer/P2H, and FC/H2P is considered. It is assumed that apart from feeding electricity demand, the DCμGO has a contract with H_2 consumers for delivery of H_2. The H_2 consumption can be for industrial applications, public transportation requirements, indoor heating, etc. [170]. Electrolyzer/P2H unit is required to generate H_2. Further, a HSS unit is incorporated to provide H_2 storage facility and increased flexibility of system operation. A FC/H2P unit is also present, which can convert H_2 to electricity if required.The smart buildings have flexible (PHEVs and TCL, i.e., air con in smart homes) and non-flexible loads. Since the DG units and flexible loads are small, they cannot participate in the energy market transactions independently. The DCμGO is an intermediary between the electricity market and individual units. The DCμG also has limited capacity. Therefore, the DCμGO behaves as a price-taker. The DCμGO collaboratively optimises power procured from the grid, power generated by the MT and H2P, H_2 production by the P2H unit, and the charging/discharging of the BESS and HSS, based on the day-ahead market price for maximising its profit while meeting all technical constraints of

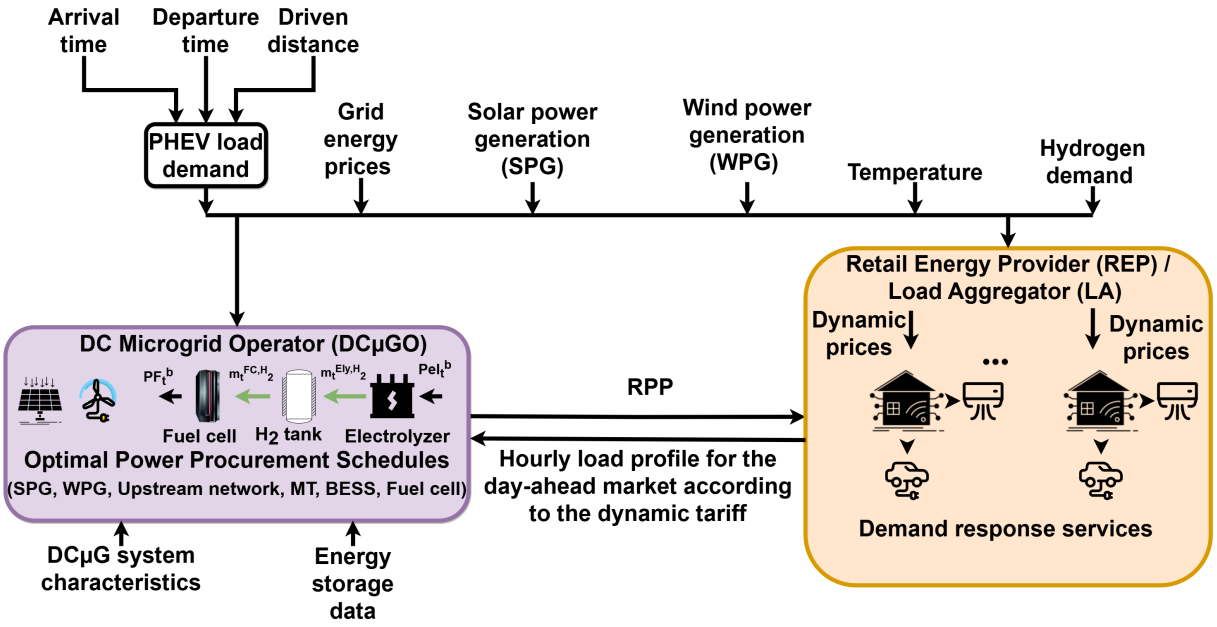

Figure 3.1: Operation framework of the EMS scheme

the DCμG network. The DCμGO also sets the RPP for the flexible and non-flexible consumers. Clusters of loads are represented by a load aggregator (LA). The LA guides the consumption pattern of individual consumers considering the user requirement and RPP to minimise the energy usage cost. The optimal load schedule is then conveyed to the DCμGO. The convergence of the DCμGO and LA objectives is achieved using an iterative privacy-preserving decentralised ADMM scheme. The operation model is shown in fig. 3.1.

3.2.2 Uncertainty Modelling

Uncertain input RVs are modelled in the probabilistic framework using pdf. Input RVs include power generation from RES, electricity and H_2 demand, grid energy price, ambient temperature, daily and subsequent trip distance of PHEVs, and their arrival and departure times. RVs related to PHEVs are assumed uncorrelated with others. Based on travel survey data of privately owned and company vehicles, it has been widely reported that the arrival and departure times of PHEVs follow Normal distributions [158, 171, 172], while daily and subsequent trip distances adhere to Log-normal distributions [130, 158, 173, 174, 175]. Therefore, we have also adopted Log-normal distribution to model daily and subsequent trip distances and Normal distribution to model the arrival and departure times of the PHEVs in this work. Existing energy content and PHEV battery power

Table 3.2: Probabilistic Uncertainty Modelling of input RVs

Parameter	Distribution	pdf	Correlated/Uncorrelated
Arrival time (t_a)	Normal	$f_{ta}(t_a) = \frac{1}{\sigma_{ta}\sqrt{2\pi}} exp\left[-\frac{(t_a-\mu_{ta})^2}{2\sigma_{ta}^2}\right]$	Uncorrelated
Departure time (t_d)	Normal	$f_{td}(t_d) = \frac{1}{\sigma_{td}\sqrt{2\pi}} exp\left[-\frac{(t_d-\mu_{td})^2}{2\sigma_{td}^2}\right]$	Uncorrelated
Driven distance (DD) (d)	Lognormal	$f_{dist}(d) = \frac{1}{d\sigma_d\sqrt{2\pi}} exp\left[-\frac{(ln(d)-\mu_d)^2}{2\sigma_d^2}\right]$	Uncorrelated
Subsequent trip distance (STD) ($d_{s,ne}$)	Lognormal	$f_{STD}(d_{s,ne}) = \frac{1}{d_{s,ne}\sigma_{ds,ne}\sqrt{2\pi}} exp\left[-\frac{\left(ln(d_{s,ne})-\mu_{ds,ne}\right)^2}{2\sigma_{ds,ne}^2}\right]$	Uncorrelated
H_2 demand ($m_t^{H_2,d}$)	Normal	$f_{H_2}(m_t^{H_2,d}) = \frac{1}{\sigma_t^{H_2,d}\sqrt{2\pi}} exp\left[-\frac{\left(m_t^{H_2,d}-\mu_t^{H_2,d}\right)^2}{2(\sigma_t^{H_2,d})^2}\right]$	Uncorrelated
WPG power (PW_t^b)	Weibull	$f_W(PW_t^b) = \frac{x_t}{c_t}\left(\frac{PW_t^b}{c_t}\right)^{(x_t-1)} \exp\left[-\left(\frac{PW_t^b}{c_t}\right)^{x_t}\right]$	Correlated
SPG power (PS_t^b)	Normal	$f_S(PS_t^b) = \frac{1}{\sigma_t^{S,b}\sqrt{2\pi}} exp\left[-\frac{\left(PS_t^b-\mu_t^{S,b}\right)^2}{2(\sigma_t^{S,b})^2}\right]$	Correlated
Non-flexible load ($PNFL_t^b$)	Normal	$f_{load}(PNFL_t^b) = \frac{1}{\sigma_t^{NFL,b}\sqrt{2\pi}} exp\left[-\frac{\left(PNFL_t^b-\mu_t^{NFL,b}\right)^2}{2(\sigma_t^{NFL,b})^2}\right]$	Correlated
Grid power price (π_t^g)	Normal	$f_{price}(\pi_t^g) = \frac{1}{\sigma_{g,t}\sqrt{2\pi}} exp\left[-\frac{\left(\pi_t^g-\mu_{g,t}\right)^2}{2(\sigma_{g,t})^2}\right]$	Correlated
Ambient temperature (F_t)	Log-normal	$f_{temp}(F_t) = \frac{1}{F_t\sigma_{F,t}\sqrt{2\pi}} exp\left[-\frac{\left(ln(F_t)-\mu_{F,t}\right)^2}{2\sigma_{F,t}^2}\right]$	Correlated

requirements are computed per [176]. Further, the Normal distribution has been used in the literature to model the forecasting error of H_2 demand [177, 178]. Hence, we have also used the Normal distribution to model the H_2 demand uncertainty in this chapter. The corresponding pdfs are shown in table 3.2.

The correlation among power outputs of SPG and WPG units, electricity demand, grid energy price, and ambient temperature is modelled utilising Copula theory. The modelling process is as follows:

- *Data processing:* Hourly data of SPG and WPG generations, inflexible electricity demand, grid price, and temperature are collected from the "ENTSO-E Transparency" and "Photovoltaic Geographic Information System (PVGIS)" platforms [179, 180] for the summer season (June-August 2020) in Sardinia, Italy, resulting in a dataset segregated hour by hour (24 hours x 92 days). Normalisation of the data is conducted with respect to the hourly peak value (excluding temperature). Various univariate distributions like Normal distribution, Weibull distribution, Beta distribution, Log-normal distribution, Poisson distribution, etc., are fitted to the data using the $fitdist$ function of MATLAB to ascertain the best fitting pdf for each correlated input RV (SPG and WPG generation, inflexible electricity demand, grid price, and ambient temperature). The fitting results indicate "$Normal$" distribution is the best choice for SPG generation, non-flexible electricity demand, and grid price. On the other hand, "$Weibull$" and "$Lognormal$" distributions are best fits

for WPG and temperature data, respectively. Therefore, we have used the best-fit distributions ascertained based on the actual data to model the uncertainties of the correlated input RVs, as shown in table 3.2.

- *Compute rank correlation coefficient:* The Kendall rank correlation coefficient (τ_t) is computed for each pair of correlated RVs using MATLAB's "*corr*" function.

- *Model correlation between RVs:* The selection of copulas from the Archimedean family (Frank, Gumbel-Hougaard, Clayton) is made to accommodate various dependence structures, with preference given to the Frank copula due to its ability to model both positive and negative dependence. For each τ_t, the Frank copula parameter (Φ_t) is determined using MATLAB's "*copulaparam*" function.

- *Map to marginal distributions:* 20,000 data couples are randomly generated for each pair of correlated RVs at each time step using the "*copularnd*" function. The generated data is then mapped back by taking the inverse of the univariate best-fit distribution.

A Monte Carlo dynamic averaging method, with $20,000$ random samples for each hour, is adopted to find the most likelihood values of hourly input RVs (both correlated and uncorrelated) [181]. The most likelihood values are fed to the EMS of the DCμG. The pdfs of the input RVs are summarised in table 3.2.

3.2.3 Problem Formulation

3.2.3.1 Market Players and System Modelling

The DCμG is represented by a graph where nodes represent buses ($b \in \mathcal{B}$), and links represent feeders ($f \in \mathcal{F}$). There are two players: the DCμGO and the consumers. However, we introduce three players for the theoretical development: suppliers/generators, consumers, and a network operator. The role of the supplier and the network operator will be merged into one (DCμGO) since the DCμGO owns DGs and storage units. Without any loss of generality, each bus comprises multiple generation sources and loads. If an entity is not present, the corresponding term is dropped. The power generation at a bus is given by:

$$P_t^{gen,b} = P_t^{grid} + PT_t^b + PF_t^b + PW_t^b + PS_t^b + PBD_t^b - PBC_t^b - Pel_t^b \quad \forall t \in \mathcal{T}, \forall b \in \mathcal{B} \quad (3.1)$$

The supplier incurs the cost of generation but receives revenue from the network operator at $\pi^R_{t,b} P^{gen}_{t,b}$. The welfare function of the supplier is given by:

$$\begin{aligned}\mathcal{W}^S_t := \pi^{H_2}_t m^{H_2,d,b}_t + \sum_b (-\pi^{ely} - \pi^{mt} PT^b_t - \pi^{fc}\delta^{fc,b}_t - \pi^w PW^b_t - \pi^s PS^b_t \\ - \pi^{bes}(PBC^b_t + PBD^b_t) - \pi^{wc} PWC^b_t - \pi^{sc} PSC^b_t)) - \pi^g_t P^{grid}_t + \sum_b \pi^{R,b}_t P^{gen,b}_t\end{aligned} \tag{3.2}$$

Subject to ($\forall t \in \mathcal{T}, \forall b \in \mathcal{B}$):

$$\begin{cases} 0 \le PS^b_t \le PS^{pu,b}_t \overline{PS}^b; \quad 0 \le PW^b_t \le PW^{pu,b}_t \overline{PW}^b \\ \underline{PT}^b \le PT^b_t \le \overline{PT}^b; \underline{P}^{grid} \le P^{grid}_t \le \overline{P}^{grid}_t; \delta^{fc}_t \underline{PF}^b \le PF^b_t \le \delta^{fc,b}_t \overline{PF}^b \\ \underline{Pel}^b_t \le Pel^b_t \le (1 - \delta^{fc}_t)(\overline{Pel}^b_t - \underline{Pel}^b_t) + \underline{Pel}^b_t; \end{cases} \tag{3.3}$$

$$PSC^b_t = PS^{avl,b}_t \overline{PS}^b - PS^b_t; \quad PWC^b_t = PW^{avl,b}_t \overline{PW}^b - PW^b_t \tag{3.4}$$

$$EB^b_t = EB^b_{(t-1)} + PBC^b_t \eta_{bc} - \frac{PBD^b_t}{\eta_{bd}} \tag{3.5}$$

$$\begin{aligned} &0 \le PBC^b_t \le \delta^{bat,c,b}_t \overline{PBC}^b; \\ &0 \le PBD^b_t \le (1 - \delta^{bat,c,b}_{t,b}) \overline{PBD}^b; \quad \delta^{bat,c,b}_t \in \{0,1\} \end{aligned} \tag{3.6}$$

$$0.2\overline{EB}^b \le EB^b_t \le \overline{EB}^b; EB^b_0 = EB^b_T \tag{3.7}$$

$$m^{Ely,H_2,b}_t = \eta_{el} \left(\frac{Pel^b_t}{Q^{H_2}_{hhv}} \right); P^{heat,b}_t = (1 - \eta_{el}) Pel^b_t \tag{3.8}$$

$$\theta^{el,b}_t = \theta^{el,b}_{t-1} + \left(\frac{P^{heat}_{t,b} - H^{loss}_{t,b} - hr^b_t}{C^{el}_{lmp}} \right) \tag{3.9}$$

$$m^{FC,H_2}_{t,b} = \frac{PF^b_t}{Q^{H_2}_{hhv}} \tag{3.10}$$

$$\underline{\theta}^{el,b} \le \theta^{el,b}_t \le \overline{\theta}^{el,b}; H^{loss,b}_t = \frac{\theta^{el,b}_t - F_t}{R^{Ely}_{heat}} \tag{3.11}$$

$$VH^b_t = VH^b_{t-1} + \left(\frac{m^{Ely,H_2,b}_t - m^{FC,H_2,b}_t - m^{H_2,d,b}_t}{\rho_{H_2}} \right) \tag{3.12}$$

$$\underline{VH}^b_t \le VH^b_t \le \overline{VH}^b_t; \quad VH^b_0 = V^H_{T,b} \tag{3.13}$$

The first term in (3.2) denotes incomes from H_2 sales. The second, third, fourth, fifth, and sixth terms denote the electrolyzer, MT, FC, WPG, and SPG power costs, respectively. The seventh term denotes the BESS operating cost. The eighth and ninth terms in (3.2) denote WPG and SPG power curtailment costs, respectively. The tenth term is the grid power cost, and the last term in (3.2) is the revenue for power generation. (3.3) denotes generation constraints. The SPG/WPG power curtailment is given in (3.4). The energy update and charging/discharging limits of the BESS are shown in (3.5) and (3.6), respectively. The DOC and DOD constraints of the BESS and its energy requirement at the end of the optimisation cycle are shown in (3.7). The mass rate of H_2 and heat produced by the electrolyzer are given by (3.8). The electrolyzer stack temperature and the mass of H_2 consumed by the FC are given by eq. (3.9) and (3.10), respectively. The volume of H_2 in the HSS is governed by (3.12). (3.13) imposes limits of H_2 storage levels and ensures the same storage level at the beginning and the end of the optimisation period.

The "network welfare function" is as follows:

$$\mathcal{W}_t^N := \sum_{b\in\mathcal{B}} [\pi_t^{R,b}(PFL_t^b + PNFL_t^b - P_t^{gen,b})] \tag{3.14}$$

Subject to ($\forall t \in \mathcal{T}, \forall b \in \mathcal{B}, \forall f \in \mathcal{F}$):

$$P_t^{inj,b} = P_t^{gen,b} - (PNFL_t^b + PFL_t^b) = P_t^{gen,b} - PL_t^b = P_{base} \sum_{n\in\mathcal{B}} G_{b,n} V_t^n V_t^b \tag{3.15}$$

$$0.95 \leq V_t^b \leq 1.05; \tag{3.16}$$

$$-\overline{\mathcal{I}}^f \leq \mathcal{I}_t^f \leq \overline{I}^f \tag{3.17}$$

(3.15) denotes the power flow equation with nodal power balance. The bus voltage and line current limits are given in (3.16) and (3.17), respectively.

The consumer welfare function is given as follows:

$$\mathcal{W}_t^C := -\sum_{b\in\mathcal{B}} \pi_t^{R,b} \left(PFL_t^b + PNFL_t^b\right) \tag{3.18}$$

Subject to ($\forall t \in \mathcal{T}, \forall b \in \mathcal{B}, \forall e \in \mathcal{E}, \forall a \in \mathcal{A}$):

$$\begin{aligned} &0 \leq PEV_{t,e}^C \leq \delta_{t,e}^{E,C} \overline{PEV}_e^C, 0 \leq PEV_{t,e}^D \leq \delta_{t,e}^{E,D} \overline{PEV}_e^D, \\ &\delta_{t,e}^{E,C} + \delta_{t,e}^{E,D} \leq 1; \quad \delta_{t,e}^{E,C} \in \{0,1\}; \quad \delta_{t,e}^{E,D} \in \{0,1\} \end{aligned} \tag{3.19}$$

$$E_{t,e}^{E} = \begin{cases} E_{e}^{AE} & : t = t_{a,e} \\ E_{(t-1),e}^{E} + PEV_{t,e}^{C}\eta_{ev}^{c} - \frac{PEV_{t,e}^{D}}{\eta_{ev}^{D}} & : t_{a,e} < t \leq t_{d,e} \end{cases} \tag{3.20}$$

$$\underline{E}_{e}^{E} \leq E_{t,e}^{E} \leq \overline{E}_{e}^{E}; E_{td,e} = E_{e}^{E,R} \tag{3.21}$$

$$\theta_{t,a}^{A,b} = \epsilon_A \theta_{(t-1),a}^{A,b} + (1 - \epsilon_A)\left(F_t - \frac{\eta_A \, PA_{t,a}^{b}}{A_{a}^{cond,b}}\right) \tag{3.22}$$

$$\underline{\theta}_{a}^{A,b} \leq \theta_{t,a}^{A,b} \leq \overline{\theta}_{a}^{A,b}; 0 \leq PA_{t,a}^{b} \leq \overline{PA}_{a}^{b} \tag{3.23}$$

$$PFL_{t}^{b} = \sum_{a \in \mathcal{A}} PA_{t,a}^{b} + \sum_{e \in \mathcal{E}} (PEV_{t,e}^{C} - PEV_{t,e}^{D}); PL_{t}^{b} = PFL_{t}^{b} + PNFL_{t}^{b} \tag{3.24}$$

The charging and discharging limits of PHEV are given by (3.19), while (3.20) is the energy update equation of the PHEV battery. The DOC and DOD constraints of the PHEV battery and its final energy requirement are shown in (3.21). The indoor temperature dynamics of a room cooled by an air con is shown in (3.22). The allowable indoor temperature and air con power limits are given by (3.23). The total flexible load comprises the sum of PHEV and air con loads, while the total load at a bus is the sum of flexible and non-flexible load (3.24).

3.2.3.2 Linearisation of non-convex DCμG network model

The equality constraint (3.15) is a non-affine equality constraint, making the network model non-convex [156]. The above non-affine equality constraint is convexified using linearisation. The DCμG is interfaced with the upstream grid through a GIC connected to bus #1 of the DCμG. The GIC maintains the bus voltage at 1.0 per unit (p.u.), while the active power exchange between the upstream grid and the DCμG network is not specified as apriori. Therefore, the bus to which the GIC is connected is treated as slack node [182]. Under normal operating conditions, bus voltages V_t^b are close to 1.0 p.u.. We can write:

$$V_{t}^{b} = 1 + \Delta V_{t}^{b}; V_{t}^{n} = 1 + \Delta V_{t}^{n}; \quad \Delta V_{t}^{b}, \Delta V_{t}^{n} << 1 \tag{3.25}$$

Therefore, we can rewrite (3.15) as follows:

$$\frac{P_t^{inj,b}}{P_{base}} = \sum_{n\in\mathcal{B}} G_{b,n} V_t^n V_t^b = \sum_{n\in\mathcal{B}} G_{b,n}(1+\Delta V_t^n)(1+\Delta V_t^b)$$
$$= \sum_{n\in\mathcal{B}} G_{b,n}(1+\Delta V_t^n + \Delta V_t^b + \Delta V_t^b \Delta V_t^n) \approx \sum_{n\in\mathcal{B}} G_{b,n}(1+\Delta V_t^n + \Delta V_t^b) \tag{3.26}$$

Since ΔV_t^n and ΔV_t^b are small, the product $\Delta V_t^b \Delta V_t^n$ is neglected in (3.26). Using (3.25) in (3.26), we obtain:

$$\frac{P_t^{inj,b}}{P_{base}} \approx \sum_{n\in\mathcal{B}} G_{b,n}(V_t^n + V_t^b - 1) = \sum_{n\in\mathcal{B}} G_{b,n} V_t^n = \sum_{n\in\mathcal{B}} G_{b,n} \Delta V_t^n \tag{3.27}$$

Since the **G**-bus matrix is symmetric, we have used $\sum_{n\in\mathcal{B}} G_{b,n} = 0$ and $\sum_{n\in\mathcal{B}} G_{b,n} V_t^b = 0$ in (3.27). Therefore, the linear power flow model, given by (3.27), will replace the non-convex power flow model given by (3.15). Note that $\Delta V_t^b = 0$ for the slack bus (i.e., bus #1). (3.27) can be written in matrix form as:

$$[\mathbf{P}_t^{inj}] = P_{base}[\mathbf{G}][\mathbf{\Delta V}_t] \tag{3.28}$$

Since $[\mathbf{G}]$ is a singular matrix, the slack bus row and column are removed to obtain an invertible matrix $[\mathbf{G}_{mod}]$. Similarly, the row corresponding to the slack bus is removed from the power injection column vector to form $\mathbf{P}_t^{mod,inj}$. We can write the following.

$$[\mathbf{\Delta V}_t^{mod}] = \frac{1}{P_{base}} [\mathbf{G}_{mod}]^{-1} [\mathbf{P}_t^{mod,inj}] \tag{3.29}$$

The slack bus row and column with all zeros are appended to $[\mathbf{G}_{mod}]^{-1}$ to form $[\mathbf{\Xi}]$. We can write the following:

$$[\mathbf{\Delta V}_t] = \frac{1}{P_{base}} [\mathbf{\Xi}][\mathbf{P}_t^{inj}] \tag{3.30}$$

Thus, the bus voltage deviation (from 1.0 p.u.) at bus #b is given by:

$$\Delta V_t^b = \frac{1}{P_{base}} \sum_{n\in\mathcal{B}} \Xi_{bn} P_{t,n}^{inj} \tag{3.31}$$

For a DCμG, we define the Generation shift distribution factor (GSDF) to quantify the impact of power injection change at bus #j on the line current $\mathcal{I}^f$ in line #f. For a line #f connected between buses #b and #n, the GSDF is defined as:

$$GSDF_{f,j} = \Delta \mathcal{I}_t^f / \Delta P_{j_t}^{inj} \tag{3.32}$$

The current in line #f is given by:

$$\mathcal{I}_t^f = (\Delta V_t^b - \Delta V_t^n) g_{bn}; \quad g_{bn} = -G_{bn} \tag{3.33}$$

Substituting $\Delta V_t^b - \Delta V_t^n$ from (3.31) in (3.33), we get:

$$\mathcal{I}_t^f = (\sum_{k\in\mathcal{B}}(\Xi_{bj} - \Xi_{nj})P_{t,j}^{inj})\frac{g_{bn}}{P_{base}} \tag{3.34}$$

Therefore, the GSDF from bus $\#j$ to line $\#f$ is:

$$GSDF_{f-j} = \frac{g_{bn}(\Xi_{bj} - \Xi_{nj})}{P_{base}} = \frac{-G_{bn}(\Xi_{bj} - \Xi_{nj})}{P_{base}} = \frac{\varpi_{f,j}}{P_{base}} \tag{3.35}$$

Therefore, the network constraints, given by (3.15), (3.16), and (3.17), can be rewritten as follows:

$$P_t^{gen,b} - (PNFL_t^b + PFL_t^b) = P_t^{gen,b} - PL_t^b = P_{base}\sum_{n\in\mathcal{B}} G_{b,n}\Delta V_t^n \quad : \text{Nodal power balance} \tag{3.36}$$

$$-\overline{\Delta V} \leq \frac{1}{P_{base}}\sum_{n\in\mathcal{B}} \Xi_{bn}(P_t^{gen,n} - PL_t^n) \leq \overline{\Delta V}; \quad \overline{\Delta V} = 0.05 \quad : \text{Bus voltage limits} \tag{3.37}$$

$$-\overline{\mathcal{I}}^f \leq \sum_{b\in\mathcal{B}} \varpi_{l,b}\left(\frac{P_t^{gen,b} - PL_t^b}{P_{base}}\right) \leq \overline{\mathcal{I}}^f \quad : \text{Line current limits} \tag{3.38}$$

Note that (3.36), (3.37), and (3.38) are linear equations describing the DCμG model and constraints.

3.2.3.3 Competitive Equilibria

Definition 1. The competitive equilibrium is a triplet of process vectors: $\{\mathbf{PL}_e, \mathbf{P}_e^{gen}, \boldsymbol{\pi}_e^R\}$; power demanded by the consumers, power supplied by the suppliers, and energy trading price satisfying the following: (a) Solve the consumer's optimisation problem to obtain the equilibrium value:

$$\mathbf{PL}_e \in \arg\max_{\mathbf{PL}} \left\langle \boldsymbol{\mathcal{W}}^C, \mathbf{1}\right\rangle ; \text{s.t.} : (3.19) - (3.24) \tag{3.39}$$

(b) Solve the supplier's optimisation problem to obtain the equilibrium value:

$$(\mathbf{P}_e^{gen}) \in \arg\max_{\mathbf{P}^{gen}} \left\langle \boldsymbol{\mathcal{W}}^S, \mathbf{1}\right\rangle ; \text{s.t.} : (3.3) - (3.13) \tag{3.40}$$

(c) Solve the network's optimisation problem to obtain equilibrium values with $\boldsymbol{\pi}_e^R$ as Lagrange multiplier associated with (3.36)-(3.38):

$$(\mathbf{PL}_e, \mathbf{P}_e^{gen}) \in \arg \max_{\mathbf{PL}, \mathbf{P}^{gen}} \left\langle \boldsymbol{\mathcal{W}}^N, \mathbf{1} \right\rangle ; \text{s.t.} : (3.36) - (3.38) \tag{3.41}$$

The suppliers and consumers satisfy the measurability constraint, i.e., they share equal information, modelled by common filtration with an increasing family of σ-algebras. We denote the same by $\mathcal{H} = \{\mathcal{H}_t : t \geq 0\}$. The price process $\boldsymbol{\pi}^R$, and decisions of the supplier $\mathbf{P}^{gen}$, and the consumer $\mathbf{PL}$ adapt to this filtration. Further, the consumer and supplier decisions and price process vector components lie in L_2. Also, no player is big enough to manipulate market price. The total welfare of the system is defined by $\mathcal{W}_t^{TOT} := \mathcal{W}_t^S + \mathcal{W}_t^C + \mathcal{W}_t^N$, and is independent of the price process.

Definition 2. The "efficient allocation" can be obtained by solving the social welfare problem (SWP) given by [183]:

$$\{ \max_{\mathbf{P}^{gen}, \mathbf{P}^L} \left\langle \boldsymbol{\mathcal{W}}^{TOT}, \mathbf{1} \right\rangle, st : (3.3) - (3.13), (3.36) - (3.38), (3.19) - (3.24)\} \tag{3.42}$$

$$\begin{aligned}
\pounds = & - \left\langle \boldsymbol{\mathcal{W}}^{TOT}, \mathbf{1} \right\rangle + \sum_{b \in \mathcal{B}} \left\langle \boldsymbol{\lambda}^b, (\boldsymbol{\Psi}^b(\mathbf{P}^{gen,b}, \mathbf{PL}^b)) \right\rangle + \sum_{f \in \mathcal{F}} \left\langle \boldsymbol{\mu}^{+,f}, (\mathbf{P}^{gen} - \mathbf{PL}) \varpi_f \frac{1}{P_{base}} - \overline{\mathcal{I}}^f \right\rangle \\
& + \sum_{f \in \mathcal{F}} \left\langle \boldsymbol{\mu}^{-,f}, -(\mathbf{P}^{gen} - \mathbf{PL}) \varpi_f \frac{1}{P_{base}} - \overline{\mathcal{I}}^f \right\rangle + \sum_{n \in \mathcal{B}} \left\langle \boldsymbol{\nu}^{+,n}, (\mathbf{P}^{gen} - \mathbf{PL}) \boldsymbol{\Xi}_n \frac{1}{P_{base}} - \overline{\Delta V} \right\rangle \\
& + \sum_{n \in \mathcal{B}} \left\langle \boldsymbol{\nu}^{-,n}, -(\mathbf{P}^{gen} - \mathbf{PL}) \boldsymbol{\Xi}_n \frac{1}{P_{base}} - \overline{\Delta V} \right\rangle
\end{aligned} \tag{3.43}$$

The solution of the SWP is $(\mathbf{P}^{gen,*}, \mathbf{P}^{L,*})$. The Lagrangian of the SWP is given in (3.43). $\boldsymbol{\Psi}$ denotes the nodal power balance. $\boldsymbol{\lambda}$ is unconstrained, $\mu_t^{+,f}, \mu_t^{-,f}, \nu_t^{+,b}, \nu_t^{-,b} \geq 0 : \forall t \in \mathcal{T}, \forall f \in \mathcal{F}, \forall b \in \mathcal{B}$. λ^b is the Lagrange multiplier associated with nodal power balance. $\mu_t^{+,f}$ and $\mu_t^{-,f}$ are the Lagrange multipliers associated with line current upper and lower limits, respectively. $\nu_t^{+,b}, \nu_t^{-,b}$ are Lagrange multipliers associated with the bus voltage upper and lower limits, respectively. Define the price process as:

$$\pi_t^{R,b} := \lambda_t^b + \sum_{f \in \mathcal{F}} (\mu_t^{-,f} - \mu_t^{+,f}) \varpi_{f,b} + \sum_{n \in \mathcal{B}} (\nu_t^{-,b} - \nu_t^{+,b}) \Xi_{n,b} \tag{3.44}$$

Substituting the value of the above in (3.43), we obtain:

$$\pounds = - \boldsymbol{\mathcal{W}}^C - \boldsymbol{\mathcal{W}}^{gen} - \sum_{f \in \mathcal{F}} \left\langle \boldsymbol{\mu}^{+,f} + \boldsymbol{\mu}^{-,f}, \overline{\mathcal{I}}^f \right\rangle - \sum_{n \in \mathcal{B}} \left\langle \boldsymbol{\nu}^{+,b} + \boldsymbol{\nu}^{-,b}, \overline{\Delta V} \right\rangle \tag{3.45}$$

The dual functional of the SWP is as follows:

$$\kappa(\boldsymbol{\lambda}, \boldsymbol{\mu}^{+}, \boldsymbol{\mu}^{-}, \boldsymbol{\nu}^{+}, \boldsymbol{\nu}^{-}) = \min_{\boldsymbol{P}^{gen}, \boldsymbol{P}^{L}} \pounds \tag{3.46}$$

Minimisation in (3.46) is equivalent to relaxation of the SWP (3.42), i.e., the weak duality bound given below holds [183].

Lemma (Weak Duality). The following holds for any allocation $\{\mathbf{P}^{gen}, \mathbf{P}^{L}\}$ and Lagrange multipliers $(\boldsymbol{\lambda}, \boldsymbol{\mu}^{+}, \boldsymbol{\mu}^{-}, \boldsymbol{\nu}^{+}, \boldsymbol{\nu}^{-})$:

$$-\left\langle \boldsymbol{\mathcal{W}}^{TOT}, \mathbf{1} \right\rangle \geq \kappa(\boldsymbol{\lambda}, \boldsymbol{\mu}^{+}, \boldsymbol{\mu}^{-}, \boldsymbol{\nu}^{+}, \boldsymbol{\nu}^{-}) \tag{3.47}$$

The equality in (3.47) should hold for strong duality.

Theorem 1.[183] If the strong duality holds for the SWP, then and only then the market admits a competitive equilibrium.

Sufficient Condition: As the strong duality holds, we have:

$$-\left\langle \boldsymbol{\mathcal{W}}^{TOT}, \mathbf{1} \right\rangle = \kappa(\boldsymbol{\lambda}, \boldsymbol{\mu}^{+}, \boldsymbol{\mu}^{-}, \boldsymbol{\nu}^{+}, \boldsymbol{\nu}^{-}) \tag{3.48}$$

Let the price be defined as in (3.44). Let $\{\mathbf{PL}, \mathbf{P}^{gen}\}$ be a feasible solution of the SWP. Therefore, the nodal power balance holds $\forall t \in \mathcal{T}$. Hence, (3.49) holds.

$$\begin{aligned}
\pounds = &-\left\langle \boldsymbol{\mathcal{W}}^{TOT}, \mathbf{1} \right\rangle + \sum_{f \in \mathcal{F}} \left\langle \boldsymbol{\mu}^{+,f}, (\mathbf{P}^{gen} - \mathbf{PL}) \varpi_f \frac{1}{P_{base}} - \overline{\mathcal{I}}^{f} \right\rangle + \\
&\sum_{f \in \mathcal{F}} \left\langle \boldsymbol{\mu}^{-,f}, -(\mathbf{P}^{gen} - \mathbf{PL}) \varpi_f \frac{1}{P_{base}} - \overline{\mathcal{I}}^{f} \right\rangle \\
&+ \sum_{n \in \mathcal{B}} \left\langle \boldsymbol{\nu}^{+,n}, (\mathbf{P}^{gen} - \mathbf{PL}) \boldsymbol{\Xi}_n \frac{1}{P_{base}} - \overline{\Delta V} \right\rangle + \sum_{n \in \mathcal{B}} \left\langle \boldsymbol{\nu}^{-,n}, -(\mathbf{P}^{gen} - \mathbf{PL}) \boldsymbol{\Xi}_n \frac{1}{P_{base}} - \overline{\Delta V} \right\rangle
\end{aligned} \tag{3.49}$$

Also, feasibility implies : $-\overline{\mathcal{I}}^{f} \leq \sum_{b \in \mathcal{B}} \varpi_{f,b} \left(\frac{P_t^{inj,b}}{P_{base}} \right) \leq \overline{\mathcal{I}}^{f}$ and $-\overline{\Delta V} \leq \sum_n \Xi_{b,n} \frac{P_t^{gen,n} - PL_t^n}{P_{base}} \leq \overline{\Delta V}$, with $\mu_t^{+,f}, \mu_t^{-,f}, \nu_t^{+,b}, \nu_t^{-,b} \geq 0 : \forall t \in \mathcal{T}, \forall f \in \mathcal{F}, \forall b \in \mathcal{B}$. Therefore,:

$$\left\langle \boldsymbol{\mu}^{+,f}, (\mathbf{P}^{gen} - \mathbf{PL})\varpi_f \frac{1}{P_{base}} - \overline{\mathcal{I}}^f \right\rangle \leq 0; \tag{3.50a}$$

$$\left\langle \boldsymbol{\mu}^{-,f}, -(\mathbf{P}^{gen} - \mathbf{PL})\varpi_f \frac{1}{P_{base}} - \overline{\mathcal{I}}^f \right\rangle \leq 0 \tag{3.50b}$$

$$\left\langle \boldsymbol{\nu}^{+,n}, (\mathbf{P}^{gen} - \mathbf{PL})\boldsymbol{\Xi}_n \frac{1}{P_{base}} - \overline{\Delta V} \right\rangle \leq 0 \tag{3.50c}$$

$$\left\langle \boldsymbol{\nu}^{-,n}, -(\mathbf{P}^{gen} - \mathbf{PL})\boldsymbol{\Xi}_n \frac{1}{P_{base}} - \overline{\Delta V} \right\rangle \leq 0 \tag{3.50d}$$

Using (3.48), $\mathcal{L} \leq \kappa(\boldsymbol{\lambda}, \boldsymbol{\mu}^+, \boldsymbol{\mu}^-, \boldsymbol{\nu}^+, \boldsymbol{\nu}^-)$, but by definition (3.46), $\mathcal{L} \geq \kappa(\boldsymbol{\lambda}, \boldsymbol{\mu}^+, \boldsymbol{\mu}^-, \boldsymbol{\nu}^+, \boldsymbol{\nu}^-)$. Hence,

$$\mathcal{L} = \kappa(\boldsymbol{\lambda}, \boldsymbol{\mu}^+, \boldsymbol{\mu}^-, \boldsymbol{\nu}^+, \boldsymbol{\nu}^-) \tag{3.51}$$

(3.51) indicates that $\mathbf{PL}$ maximises the welfare of the consumers and $\mathbf{P}^{gen}$ maximises the welfare of the supplier. Moreover, equalities hold in (3.50). Further, with the prices defined in (3.44), the optimisation objective of the network becomes:

$$\left\langle \sum_{f \in \mathcal{F}} (\boldsymbol{\mu}^{+,f} + \boldsymbol{\mu}^{-,f})\overline{\mathcal{I}}^f, \mathbf{1} \right\rangle + \left\langle \sum_{n \in \mathcal{B}} (\boldsymbol{\nu}_b^+ + \boldsymbol{\nu}_b^-)\overline{\Delta V}, \mathbf{1} \right\rangle \tag{3.52}$$

The objective of the network is independent of $\mathbf{P}^{gen}$ and $\mathbf{PL}$, i.e., the price $\boldsymbol{\pi}^R$ maximises the network welfare and is the equilibrium price. Therefore, $\{\mathbf{P}^{gen}, \boldsymbol{\pi}^R, \boldsymbol{\pi}^R\}$ forms a competitive equilibrium.

Necessary Condition: Let $\{\mathbf{P}_e^L, \mathbf{P}_e^{gen}, \boldsymbol{\pi}_e^R\}$ be a competitive equilibrium. Note that $\{\mathbf{P}_e^L, \mathbf{P}_e^{gen}\}$ maximises the welfare of the network is the price is $\boldsymbol{\pi}_e^R$. The corresponding Lagrangian is given in (3.53):

$$\begin{aligned}
\mathcal{L}_N = &- \sum_{b \in \mathcal{B}} \left\langle \boldsymbol{\pi}_e^{R,b}(\mathbf{PL}_e^b - \mathbf{P}_e^{gen,b}) \right\rangle + \sum_{b \in \mathcal{B}} \left\langle \boldsymbol{\lambda}^b, (\boldsymbol{\Psi}_b(\mathbf{P}_e^{gen,b}, \mathbf{PL}_e^b)) \right\rangle \\
&+ \sum_{f \in \mathcal{F}} \left\langle \boldsymbol{\mu}^{+,f}, (\mathbf{P}_e^{gen} - \mathbf{PL}_e)\varpi_f \frac{1}{P_{base}} - \overline{\mathcal{I}}^f \right\rangle + \sum_{f \in \mathcal{F}} \left\langle \boldsymbol{\mu}^{-,f}, -(\mathbf{P}_e^{gen} - \mathbf{PL}_e)\varpi_f \frac{1}{P_{base}} - \overline{\mathcal{I}}^f \right\rangle \\
&+ \sum_{n \in \mathcal{B}} \left\langle \boldsymbol{\nu}^{+,n}, (\mathbf{P}_e^{gen} - \mathbf{PL}_e)\boldsymbol{\Xi}_n \frac{1}{P_{base}} - \overline{\Delta V} \right\rangle + \sum_{n \in \mathcal{B}} \left\langle \boldsymbol{\nu}^{-,n}, -(\mathbf{P}_e^{gen} - \mathbf{PL}_e)\boldsymbol{\Xi}_n \frac{1}{P_{base}} - \overline{\Delta V} \right\rangle
\end{aligned} \tag{3.53}$$

The optimum $\{\mathbf{PL}_e, \mathbf{P}_e^{gen}\}$ satisfies KKT criteria since it is a linear program. Hence, for constraints $\frac{\partial \mathcal{L}_N}{\partial PL^b} = \frac{\partial \mathcal{L}_N}{\partial P^{gen,b}} = 0$, $\exists\{\boldsymbol{\lambda}, \boldsymbol{\mu}^+, \boldsymbol{\mu}^-, \boldsymbol{\nu}^+, \boldsymbol{\nu}^-\}$, such that: $\pi_{t,e}^{R,b} = \lambda_t^b + \sum_{f \in \mathcal{F}}(\mu_t^{-,f} -$

$\mu_t^{+,f})\varpi_{f,b} + \sum_{n\in\mathcal{B}}(\nu_t^{-,b} - \nu_t^{+,b})\Xi_{n,b}\ \forall t \in \mathcal{T}, \forall b \in \mathcal{B}$. In other words, the equilibrium price $\boldsymbol{\pi}_e^b$ satisfies (3.44). Let the dual function $\kappa(.)$ of the SWP be formulated with Lagrange multipliers from the networks optimisation problem. With the form (3.44) for the price process, the following follows:

$$\{\mathbf{P}_e^L, \mathbf{P}_e^{gen}\} \in \arg\min_{\mathbf{PL},\mathbf{P}^{gen}} \pounds \tag{3.54}$$

Substitution of $\{\mathbf{P}_e^L, \mathbf{P}_e^{gen}\}$ into (3.43) and application of complementary slackness criteria associated with (3.53), we obtain the following:

$$-\left\langle \boldsymbol{\mathcal{W}}^{TOT}, \mathbf{1} \right\rangle = \kappa(\boldsymbol{\lambda}, \boldsymbol{\mu}^+, \boldsymbol{\mu}^-, \boldsymbol{\nu}^+, \boldsymbol{\nu}^-) \tag{3.55}$$

In other words, the strong duality holds. Since only the optimal Lagrange multipliers lead to strong duality, we obtain the following corollary.

Corollary 1. *The price given in* (3.44) *with optimal Lagrange multipliers is the only candidate for prices in a competitive equilibrium.*

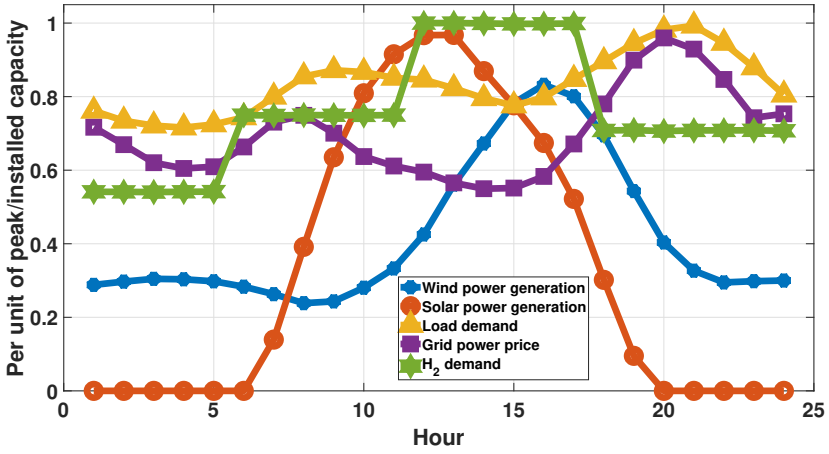

Figure 3.2: Hourly most likelihood values of WPG, SPG, load, price, and H_2 demand

3.2.4 Reformulation and Solution

The RPP is set as per Corollary 1. The roles of the supplier and the network operator are merged into one (DCμGO), and the welfare function of the DCμGO is given by $\mathcal{W}_t^{DC\mu GO} = \mathcal{W}_t^S + \mathcal{W}_t^N$. The objective of the DCμGO is to maximise the profit ($\mathcal{W}_1$):

Table 3.3: Test System Data

GIC:	Bus #1, $\underline{P^{grid}} = -25kW$, $\overline{P^{grid}} = 25kW$;
BESS:	Bus #2, $\eta_{bc}/\eta_{bd} = 95\%$, $\underline{PBC} = 0kW$, $\overline{PBC} = 15kW$ $\underline{PBD} = 0kW$, $\overline{PBD} = 15kW$, $\underline{EB} = 6kWh$, $\overline{EB} = 30kWh$ $EB_0 = 18kWh$, $\pi^{bes} = 0.006\$/kWh$;
FC:	Bus #3, $\underline{PF} = 5kW$, $\overline{PF} = 50kW$, $\pi^{fc} = 0.133\$/kWh$;
Electrolyzer/P2H & **HSS:**	Bus #3, $\underline{Pel} = 6.5kW$, $\overline{Pel} = 100kW$, $\pi^{ely} = 0.107\$$ $\eta_{el} = 0.68$, $\varrho_{H_2} = 7.8kg/m^3$, $R^{EL}_{heat} = 18°C/kW$, $C^{el}_{lmp} = 0.0833MW/°C$, $Q^{H_2}_{hhv} = 39.4kWh/kg$, $\underline{VH} = 0.25Nm^3$, $\overline{VH} = 2.0Nm^3$, $VH_0 = 0.9Nm^3$, $\pi^{H_2} = 5\$/kg$;
WPG:	Bus #3, $\overline{PW} = 100kW$, $\pi^{wc} = 0.2\$/kW$, $\pi^{w} = 0.0342\$/kW$;
SPG:	Bus #3, $\overline{PS} = 100kW$, $\pi^{sc} = 0.2\$/kW$, $\pi^{s} = 0.0274\$/kW$;
MT:	Bus #6, $\overline{PT} = 50kW$, $\underline{PT} = 0kW$, $\pi^{mt} = 0.16144\$/kW$;
TCL parameters:	$\epsilon_A = 0.93$, $\eta_A = 2.5$, $\overline{PA} = 3.5kW$, $\underline{\theta}^A_a = 75.20°F$, $\overline{\theta}^A_a = 80.6°F$, $\theta^A_{0,a} = 77°F$;
PHEV:	$\eta^C_{ev}/\eta^D_{ev} = 95\%$;

$$\begin{aligned} &\max(\mathcal{W}_1); i.e., \min(-\mathcal{W}_1); \mathcal{W}_1 = \sum_{t\in\mathcal{T}} \mathcal{W}^{DC\mu GO}_t \\ &\text{s.t.} : (3.3) - (3.13); (3.36) - (3.38) \end{aligned} \tag{3.56}$$

The objective of the consumers/LA is to minimise the cost of energy use, and is

defined as follows:

$$\min \mathcal{W}_2; \mathcal{W}_2 = \sum_{t \in \mathcal{T}} -\mathcal{W}_t^C; \text{s.t.} : (3.19) - (3.24) \tag{3.57}$$

The DVs for the DCμGO (ξ) and the LA (ϑ) are as follows:

$$\xi_t^b = \{\hat{PFL}_t^b, PT_t^b, \delta_t^{fc,b}, PW_t^b, PS_t^b, PBC_t^b, PBD_t^b, P_t^{grid}, PF_t^b, Pel_t^b, \delta_t^{bat,c,b}, hr_t^b\} \tag{3.58}$$

$$\vartheta_t^b = \{PEV_{t,e}^C, PEV_{t,e}^D, PA_{t,a}^b, \delta_{t,e}^{E,C}, \delta_{t,e}^{E,D}, PFL_t^b\} \tag{3.59}$$

The optimisation problems of the DCμGO and the LA are solved in a decentralised fashion using ADMM. The DCμGO sets the RPP and proposes load demands for every hour to the LA ($\hat{PFL}_t^b$). The LA considers the RPP as a parameter, schedules the flexible load demand (PFL_t^b), and conveys the information to DCμGO. The iterative algorithm continues until a consensus is achieved between the load values proposed by the DCμGO and the LA. The coupling constraint is given by:

$$\hat{PFL}_t^b - PFL_t^b = 0 \ : \forall t \in \mathcal{T}, \forall b \in \mathcal{B} \tag{3.60}$$

The augmented Lagrangian is defined as follows:

$$\pounds_\rho(\boldsymbol{\xi}, \boldsymbol{\vartheta}, \boldsymbol{\mu}) = -\mathcal{W}_1(\boldsymbol{\xi}) + \mathcal{W}_2(\boldsymbol{\vartheta}) + \sum_{t \in \mathcal{T}} \sum_{b \in \mathcal{B}} \mu_t^b (\hat{PFL}_t^b - PFL_t^b) + \frac{\rho}{2} \sum_{t \in \mathcal{T}} \sum_{b \in \mathcal{B}} \left\| \hat{PFL}_t^b - PFL_t^b \right\|_2^2 \tag{3.61}$$

ADMM follows the following steps:

$$\begin{aligned}
\boldsymbol{\xi}^{(i+1)} &= \arg\min_{\boldsymbol{\xi}} \pounds_\rho(\boldsymbol{\xi}, \boldsymbol{\vartheta}^{(i)}, \boldsymbol{\mu}^{(i)}) \\
\boldsymbol{\vartheta}^{(i+1)} &= \arg\min_{\boldsymbol{\vartheta}} \pounds_\rho(\boldsymbol{\xi}^{(i+1)}, \boldsymbol{\vartheta}, \boldsymbol{\mu}^{(i)}) \\
\mu_t^{(i+1),b} &= \mu_t^{(i),b} + \rho(\hat{PFL}_t^b - PFL_t^b) \ : \forall t \in \mathcal{T}, \forall b \in \mathcal{B}
\end{aligned} \tag{3.62}$$

Where $\rho > 0$: step size, μ_t^b: dual variable, i: iteration number, $\boldsymbol{\xi}$: vector of ξ_t^b, $\boldsymbol{\vartheta}$: vector of ϑ_t^b, $\boldsymbol{\mu}$: vector of μ_t^b.

Table 3.4: Scenarios

Scenarios	DR	HSS	Bi-directionality of GIC
S0	✗	✗	✗
S1	✓	✓	✓
S2	✗	✓	✓
S3	✓	✗	✓

3.3 Results and Discussion

3.3.1 Test System and Input Data

A modified version of the 6−bus 7−line DCμG system is considered [61]. The power and voltage bases are 250 kW and 380 V, respectively. The line data is available in [61]. Each line has a current rating of 0.20 p.u.. A GIC is connected to bus #1, while a BESS unit is connected to bus #2. WPG, SPG, FC, and electrolyzer are connected to bus #3. A MT is connected to bus #6. Two residential community buildings, comprising flexible and non-flexible demands, are connected to buses #4 and #5. The peak demands of the non-flexible loads at bus #4 and #5 are 12.50kW and 25kW, respectively. Each building has 10 PHEVs. The driving patterns and other parameters of PHEVs are taken from [173, 176]. We have considered four types of PHEVs as reported in [158]. The peak value of the day-ahead energy price is 0.180 \$/kWh, while the maximum H_2 demand in a day is 0.7427 kg. Other system parameters are given in table 4.2 [78, 184]. Hourly data of WPG, SPG, load demand, and grid energy price are adopted from the ENTSO-E Transparency Platform for Sardinia, Italy [179]. The hourly temperature is taken from Photovoltaic Geographic Information System (PVGIS) platform for the Sardoic summer [180] and scaled up by 50% to fit into the problem. Hourly patterns of available power from RES, non-flexible load demand, H_2 demand, and day-ahead grid energy price are shown in fig. 3.2. The ADMM step size (ρ) is taken as 0.1. The codes are written on a desktop with an Intel(R) Core(TM) $i7-9700$ CPU @3.00GHz and 16GB RAM. The uncertainty modelling is done using MATLAB 2022. The optimisation problem is formulated in General Algebraic Modeling System (GAMS) and solved with a DICOPT solver. The ADMM algorithm is terminated when $\max_{t,b} \|P\hat{F}L_t^b - PFL_t^b\| \leq 1 \times 10^{-6}$. The ADMM algorithm converges

Table 3.5: Benefits of the proposed approach

Entity	Performance Index	Scenarios			
		S0	**S1**	**S2**	**S3**
DCMGO	**Income from elec sales ($/day)**	114.47	108.97	114.99	108.23
	Income from H_2 sales ($/day)	67.41	67.41	67.41	67.41
	Operating cost ($/day)	166.01	147.65	153.62	158.95
	Profit ($/day)	15.87	28.72	28.77	16.69
Consumer	**Consumer elec cost ($/day)**	114.47	108.97	114.99	108.23
DCMGO	**% Reduction in operating cost**	NA	11.06	7.46	4.25
	% Increase in profit	NA	80.97	80.97	5.16
Consumer	**% Reduction in energy cost**	NA	4.80	-0.45	5.45

Table 3.6: Impact of flexibilities on economics

Entity	Performance Index	Scenarios		
		S1	**S2**	**S3**
DCμGO	**Income from elec sales ($/day)**	108.97	114.99	108.23
	Income from H_2 sales ($/day)	67.41	67.41	67.41
	Operating cost ($/day)	147.65	153.62	158.95
	Profit ($/day)	28.72	28.77	16.69
Consumer	**Energy cost ($/day)**	108.97	114.99	108.23
DCμGO	**% Increase in operating cost**	NA	4.04	7.65
	% decrease in profit	NA	-0.17	41.89
Consumer	**% Increase in energy cost**	NA	5.52	-0.68

in 2.707 seconds for the understudy system.

3.3.2 Simulation Results

Different scenarios are given in table 3.4. The descriptions of the scenarios are as follows:

1. *Scenario#S0:* Scenario #S0 is the base case scenario in which flexibilities of DR participators, HSS, and bi-directionality of GIC are not leveraged. Since flexible consumers do not participate in the DR program, the PHEVs adopt a dumb charging policy. In other words, a PHEV starts charging with rated charging power immediately after entering the parking lot and continues charging till the energy

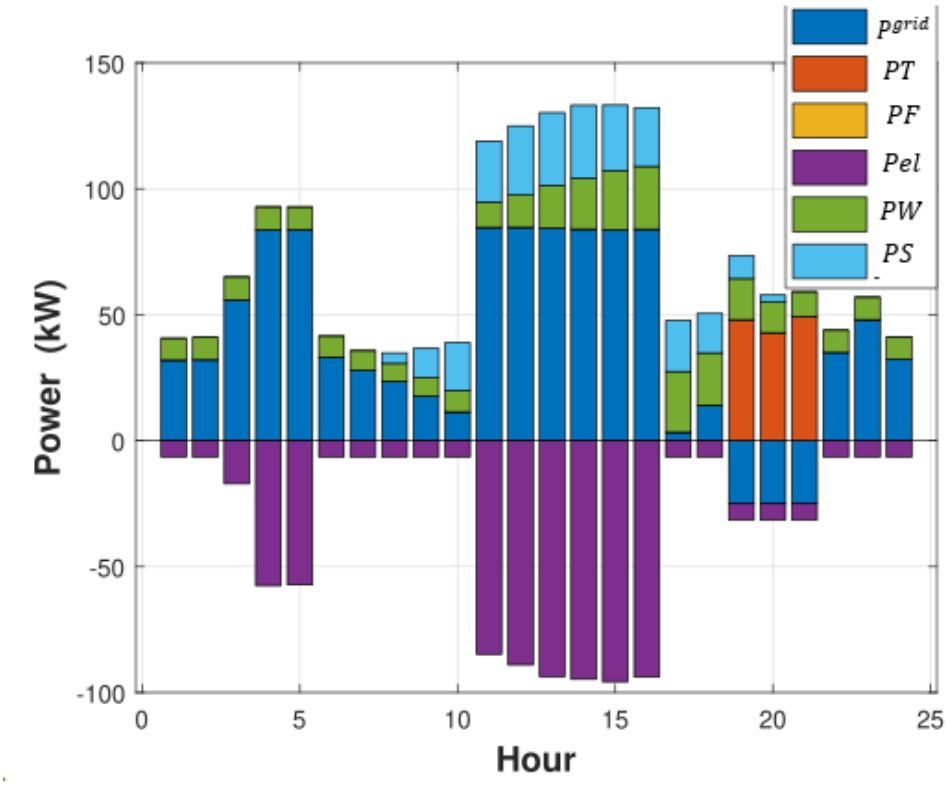

Figure 3.3: Optimal power profile

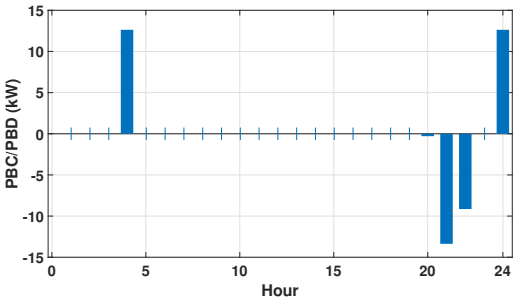

Figure 3.4: Hourly battery profile

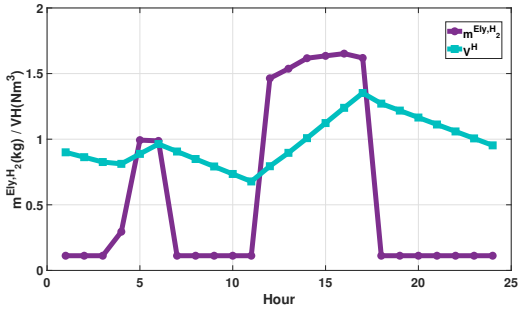

Figure 3.5: Hourly H_2 generation by electrolyzer and HSS status

requirement is met. The TCLs operate to tightly regulate the indoor room temperature between 76.95°F and 77.05°F. Moreover, the HSS is not considered in this scenario. Also, the DCμG can only procure power from the upstream grid but cannot sell power to the upstream grid.

2. *Scenario#S1:* The flexibility of DR participation is coordinated with DCμGO side flexibilities (HSS and BESS) in this scenario. The DCμGO sets the RPP according to the method proposed in this work, and flexible consumers modify the con-

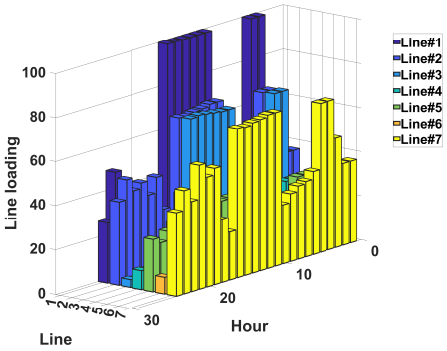

Figure 3.6: Hourly % line loading

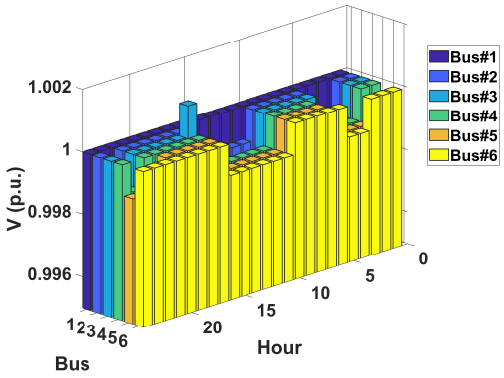

Figure 3.7: Hourly bus voltages

sumption pattern to minimise the electricity usage cost. The coordination between the DCμGO and flexible consumers is achieved using the ADMM algorithm in a privacy-preserving decentralised framework. Further, the DCμGO has the flexibility to purchase power from the upstream grid and sell power to the upstream grid.

3. *Scenario#S2:* In scenario S#2, the DR program is not activated. The behaviour of the consumers is the same as in scenario S#0. However, the HSS and the bi-directionality of the GIC are considered.

4. *Scenario#S3:* The RPP-based DR participation and bi-directionality of the GIC are considered in this scenario. However, the HSS is not present.

Scenario #S1 is adopted and proposed in this chapter. Other scenarios are for comparison.

3.3.2.1 Economic benefits of the proposed approach

Scenario $\#S0$ is the base case, where flexibilities of consumers and HSS are not considered. In other words, the DR program is not activated. The PHEVs charge according to dumb charging policy, while the TCLs maintain the indoor temperature between 76.95°F and 77.05° F. Further, the DCμG can buy power from the main grid but cannot sell power to the main grid. Both consumer and DCμGO side flexibilities are incorporated in scenario $\#S1$. The power trading between the DCμGO and the consumers occurs at RPP rates. A comparison of economic performances of different scenarios is given in table 3.5. The operating cost of DCμGO is $\sim$ 11.06% lower, while the profit is $\sim$ 80.97% higher with

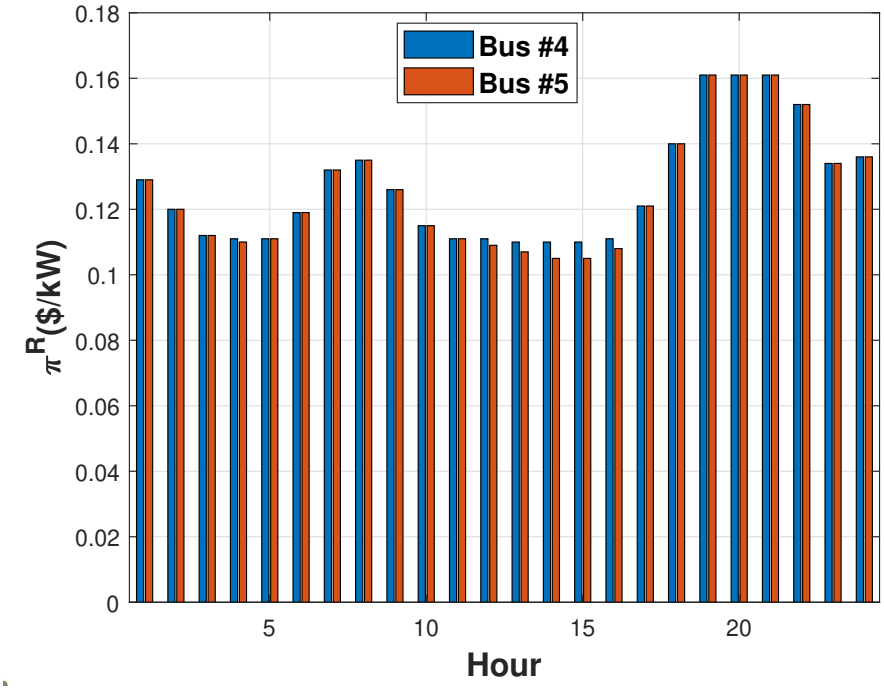

Figure 3.8: Hourly RPP

the proposed approach. The consumers also benefit by participating in the DR program since the cost of energy use in a day reduces by $\sim 4.80\%$ with the proposed approach. For scenario $\#S2$, the operating cost is $\sim 7.46\%$ lower than scenario $\#S0$, while the profit is $\sim 80.97\%$ higher. Similarly, for scenario $\#S3$, the operating cost is $\sim 4.25\%$ lower, and the profit is $\sim 5.16\%$ higher than scenario $\#S0$. Also, by participating in the DR program, the cost of energy use in a day reduces by $\sim 5.45\%$ compared to scenario $\#S0$. The operating cost, representing the negative of social welfare, is minimum in scenario $\#S1$.

3.3.2.2 Analysis of the proposed approach (Scenario $\#S1$)

The optimal schedule of power procured from the upstream grid, MT, FC, WPG, SPG, and the power demanded by the electrolyzer is shown in fig. 3.3. Electrolyzer power is shown as negative since it is a load. Negative grid power indicates that the DCμGO sells power to the grid. At all times except hours $\#19 - \#21$, power is imported from the upstream grid, and the MT remains off. It is because the day ahead power price is lower than the power generation cost of the MT. However, the grid power price increases during hours $\#19 - \#21$. Therefore, it is economical to generate power using the MT and

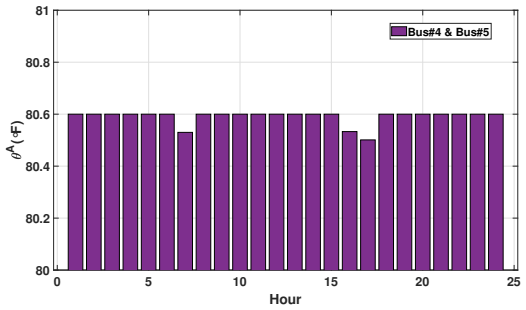

(a) Indoor temperature

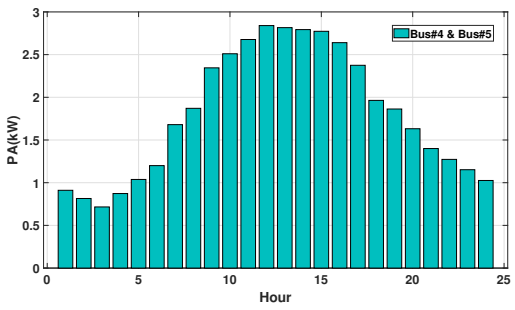

(b) Power consumption of each TCL

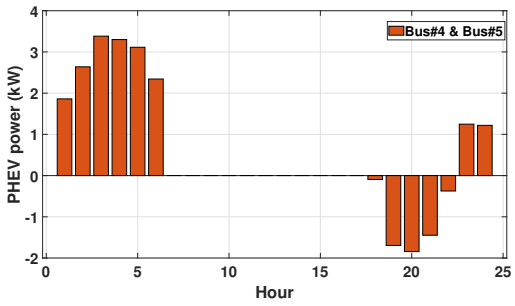

(c) PHEV power

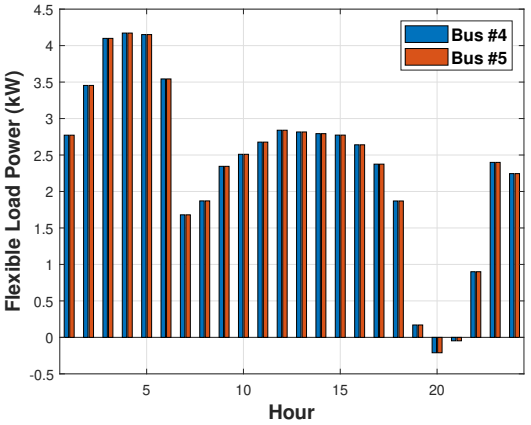

(d) Flexible power

Figure 3.9: Demands of flexible loads

sell power to the grid during this period (see fig. 3.3). RES (WPG and SPG) power is not curtailed. Further, no power is generated using the FC since two-stage conversion is involved (electricity-H_2-electricity), and the efficiency of the electrolyzer is comparatively low.

The optimal BESS profile is shown in fig. 3.4. Positive and negative powers indicate charging and discharging, respectively. The BESS charges during hour #3 and hour #23. The day-ahead grid power price is low during the aforementioned times. The BESS discharges to support the DCμGO operation at peak hours #19 and #21 when the grid power price is high. Therefore, the BESS provides arbitrage benefit. H_2 produced by the electrolyzer and the storage status of the HSS for every hour are shown in fig. 3.5. The electrolyzer demands comparatively higher power during hours $\#3 - \#5$ and $\#11 - \#16$ when the grid power price is low to generate enough H_2 for feeding the consumers and charging the HSS (see fig. 3.3 and fig. 3.5). As the day-ahead grid power price increases during the evening hours (see fig. 3.2), the electrolyzer demands minimum power during

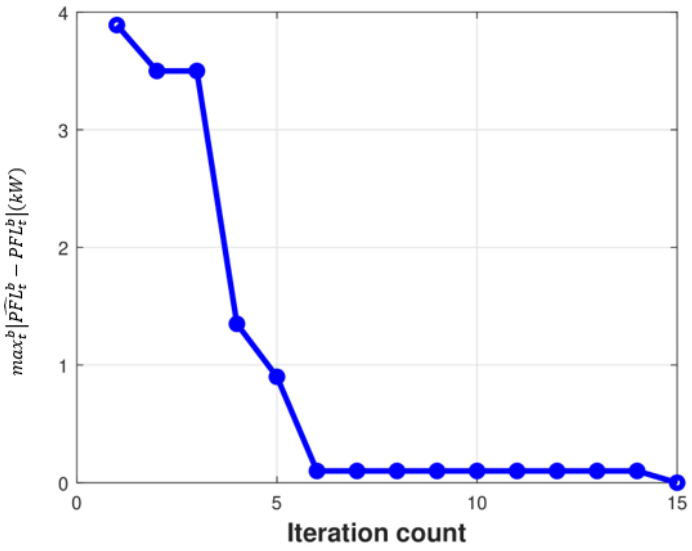

Figure 3.10: Convergence Characteristics

hours #17 − #24 (see fig. 3.3). The H_2 demand of the consumers is met by discharging the HSS during these hours, while the electrolyzer generates only a small quantity of H_2 to minimise the electrical load of the DCμG (see fig. 3.5). Therefore, the HSS provides additional flexibility in the multi-energy vector DCμG.

The hourly loading of the DCμG feeders is shown in fig. 3.6. Line #1 (connecting bus #1, i.e., the grid and bus #2) is most heavily loaded at hours #4−#5 and #11−#16 ($\sim$ 100%) since large quantities of power are imported from the grid during these periods. Other lines are loaded well below their thermal limits. Bus voltages are shown in fig. 3.7, from which it is evident that all bus voltages are tightly regulated and maintained close to the nominal value. The RPP at load buses #4 and #5 are shown in fig. 3.8. The hourly power profiles of flexible loads (PHEV and TCL) after DR implementation are shown in fig. 3.9. The PHEV operates in V2G mode during peak hours #18 − #22 when the non-flexible demand and the RPP are high (fig. 3.9c). PHEVs operate in grid-to-vehicle (G2V) mode (i.e., charge) during off-peak hours #23 − #24 and #1 − #6 since the non-flexible demand and RPP are low. The air cons consume relatively higher power during hours #7 − #17 when the non-flexible demand and RPP are low to cool the rooms. The TCL reduces power consumption during the evening and night hours (i.e., hours #18 − #24) and utilises the thermal inertia of the rooms to maintain the indoor temperature at the upper acceptable limit of 80.6° F (fig. 3.9b). Therefore, the thermal inertia of the room is also utilised in the DR implementation. The indoor temperature profile of a room is

shown in fig. 3.9a. The hourly flexible demand is shown in fig. 3.9d. The flexible demand is quite low during peak hours $\#17 - \#19$ (negative during hours $\#19 - \#21$ due to V2G operation of PHEVs). The convergence time of the ADMM algorithm is 2.707 seconds for the understudy system. The convergence characteristic is shown in fig. 3.10.

3.3.2.3 Impact of flexibilities on operation economy

Scenarios $\#S2$ and $\#S3$ are considered to investigate the financial impact of DR scheme implementation and HSS. Results are summarised in table 3.6.

- *Scenario $\#S2$ (Impact of DR):* The PHEVs operate in dumb charging mode while the indoor temperature is tightly regulated within the band of 76.95° F and 77.05° F. In other words, the flexibility of thermal inertia and PHEVs are not considered. The energy cost of the consumers increases by $\sim 5.52\%$ since the consumers cannot take advantage of the time-varying power cost. On the other hand, the operating cost of the DCμGO increases by $\sim 4.04\%$, and its profit is almost the same (slight reduction by $\sim 0.17\%$). Note that this work aims to maximise social welfare (i.e., reduce the operating cost of the DCμGO). The operating cost of the DCμGO increases since the DCμGO has to purchase greater amounts of power from the grid during peak hours (at a high day-ahead price) in the absence of flexible shiftable loads.

- *Scenario $\#S3$ (Impact of HSS):* The operating cost of the DCμGO is $\sim 7.65\%$ higher, while its profit is $\sim 41.89\%$ lower. The energy cost of consumers remains almost the same as in scenario $\#S1$. The operating cost of the DCμGO increases since the electrolyzer consumes higher amounts of electric power to generate sufficient H_2 to meet the H_2 demand during peak hours. The HSS allows the electrical power demand of the electrolyzer to be shifted from peak to off-peak hours. However, the benefit of the HSS cannot be leveraged in this scenario, leading to higher operating costs of the DCμGO. Therefore, HSS also provides electrical load-shifting flexibility and lower operating costs.

The most economical performance of the system is achieved when the flexibility of PHEVs, the thermal inertia of buildings (i.e.,TCL), and the electrical load shifting potential of HSS are coordinated to form an IDR entity in a multi-energy vector DCμG.

3.4 Conclusions

This chapter proposes a decentralised EMS using RPP-based DR implementation for an electricity-H_2 community DCμG. The DCμG operates in grid-connected mode and consists of RES, BESS, MT, P2H, H2P, and HSS. The DCμG caters to community-building loads with non-flexible (PHEV and TCL) and flexible demands. Input uncertainties, including correlation between uncertain input RVs, are modelled using Frank Copula and incorporated into the EMS utilising Monte Carlo simulations. The DCμGO sets the RPP and a proposed consumption pattern. The consumers schedule flexible load according to the RPP set by the DCμGO and the consumption pattern proposed by the DCμGO. The ADMM algorithm is used for a decentralised solution strategy to preserve players' privacy. Simulation results on a six-bus test system illustrate that there is $\sim 4.80\%$ reduction in electricity usage expense of consumers, $\sim 11.06\%$ reduction in the operating cost of the DCμGO, and $\sim 80.97\%$ increase in the DCμGO profit with the proposed EMS with IDR implementation. Forsaking the flexibility of HSS enhances the DCμGO operating cost by $\sim 7.65\%$. On the other hand, the energy usage cost of the consumers and the operating cost of the DCμGO increase by $\sim 5.52\%$ and $\sim 4.04\%$, respectively, if flexibilities of the thermal inertia of buildings and PHEVs are not incorporated in the EMS.